Rapid and sensitive detection of pyrimethanil residues on pome fruits by surface enhanced Raman scattering

Rapid and sensitive detection of pyrimethanil residues on pome fruits by Surface Enhanced Raman Scattering

Luisa Mandrile[a,b], Andrea Mario Giovannozzi[a,*], Francesca Durbiano[a], Gianmario Martra[b], Andrea Mario Rossi[a]

[a] *Division of Metrology for Quality of Life, Istituto Nazionale di Ricerca Metrologica, Strada delle Cacce, 91 10135 Torino, Italy*

[b] *Department of Chemistry and Interdepartmental Centre NIS, University of Turin, Via Giuria 7, 10125 Turin, Italy*

Food Chemistry

http://dx.doi.org/10.1016/j.foodchem.2017.10.003

Abstract

Surface Enhanced Raman Scattering (SERS) supported by gold nanoparticles (AuNPs) was applied to detect and quantify residues of pyrimethanil on pome fruits, a widely used fungicide in horticultural species. Spheroidal AuNPs with different size were fabricated and compared in this study. The analytical procedure was set up on a silicon dioxide flat substrate to standardize SERS methodology. A Raman mapping strategy was exploited to increase signal reproducibility and to minimize bias due to different local surface morphologies. Univariate and multivariate regressions were compared for calibration. Multivariate PLS approach demonstrated acceptable repeatability and method stability (RMSECV = 4.79 ppm; RMSEP = 4.31 ppm) in the range 0–40 mg kg−1, providing higher accuracy and intra-day repeatability with a mean percentage error of 18.7% and 32.8% for PLS and univariate calibration, respectively. The method here proposed can be reliably applied for PMT detection on pome fruits within the European law limits.

Keywords: Pyrimethani lPome fruit, Surface Enhanced Raman Scattering, Raman spectroscopy, Gold nanoparticles, Partial Least Squares

1. Introduction

In the last decades food safety incidents have raised public concern about synthetic additives and chemical contaminants in food, the latter of them are mainly agricultural and environmental, chemical adulterants, mycotoxins, and foreign food components (Zheng & He, 2014). Agrochemical products such as pesticides and fungicides are normally applied to protect food crops from the pests at various stages of cultivation and during post-harvest storage (Sharma, Singh, & Singh, 2009), but their intensive use can generate residues that may become a potential risk for both public health and environment (Gilden, Huffling, & Sattler, 2010). Pyrimethanil [(PMT), N-(4,6-dimethylpyrimidin-2-yl)-phenylamine] is a fungicide belonging to the anilinopyrimidine class of pesticides which inhibits the secretion of hydrolytic enzymes by the fungi during the infection process, thus stopping penetration and development of the disease (FAO, 2007). This broad spectrum fungicide is effectively used for the control of gray mould, leaf scab and other postharvest diseases on pome fruits, vegetables and ornamentals (Yu et al., 2013). Even if PMT demonstrated low acute toxicity in mammals, long-term studies showed certain toxicity in mice, rats, dogs and aquatic organisms with potential carcinogenicity. Owing to its toxicity and wide application on horticultural species, PMT has been included as a pesticide by the Commission Directive 2006/74/EC of August 2006 with a maximum residue level of 7 mg kg−1 on pome fruits (Regulation (EC) No 396/2005). Most of the published methods for the determination of PMT on fruits, vegetables and other samples are usually based on GC (Amvrazi & Tsiropoulos, 2009), GC-MS/MS (Raeppel et al., 2011, Rodriguez-Cabo et al., 2011), GC-MS (Gonzalez-Rodriguez, Rial-Otero, Cancho-Grande, & Simal-Gandara, 2008) LC-MS (Park et al., 2010), HPLC (Zhou et al., 2011), and LC-MS/MS (Ortelli, Edder, & Corvi, 2004). These methods have high accuracy, good reproducibility and provide quantitative determination of PMT according to the EU limits, but they also suffer from inevitable disadvantages such as expensive experimental instruments, trained personnel and time-consuming extraction steps. Therefore, the development of more rapid and user friendly methods for PMT residues detection on horticultural species is highly required.

2. Material and methods

2.1. Reagents and materials

Hydrogen tetrachloroaurate trihydrate (HAuCl4 3H2O ≥99%), trisodium citrate dihydrate (≥99%), were purchased from Sigma-Aldrich (Milan, Italy). Sodium hydroxide (NaOH 97%), Hydrochloric acid (HCl 37%), Nitric acid (HNO3 68%), absolute ethanol (99.99%), acetone (99,99%) and Hydroxylamine Hydrochloride (H3NO·HCl, 99+%) were obtained by Novachimica (Milano, Italy). Scala® (400 g/l of Pyrimethanil suspension) was purchased from BASF Italia (Volpiano, Italy). All solutions were prepared with Milli-Q quality water (18 MΩcm). Silicon wafers with a 300 nm of Silicon dioxide layer on top were purchased from

Si-Mat (Kaufering, Germany). Apples used for the assays were purchased in a local supermarket in Torino, Italy.

2.2. Gold nanoparticles preparation

All glassware used in the experiment was soaked in aqua regia ($HCl:HNO_3$ 3:1 v/v) and rinsed thoroughly in water and dried with nitrogen prior to use. Spheroidal AuNPs with a diameter of about 30 nm, 40 nm and 55 nm were synthesized according to Frens, 1973. Briefly, 7 ml, 5 ml and 3.5 ml of a 1% aqueous solution of trisodium citrate were rapidly injected into 500 ml boiling solution of HAuCl4 (0.01% v/v) for the preparation of 30 nm, 40 nm and 55 nm AuNPs, respectively. The mixture was further refluxed for 10 min and then cooled to room temperature under continuous stirring. Larger AuNPs with a diameter of 90 nm and 120 nm were obtained via seed-mediated growth of 30 nm and 40 nm AuNPs, respectively, using an optimized growing procedure based on hydroxylamine hydrochloride (Li et al., 2013). In detail, 4 ml of Au seeds suspension were put into a round-bottom flask with 53.8 ml of Milli-Q water under continuous stirring and the different solutions were added in the following order: 920 µl of 1% v/v aqueous solution of trisodium citrate (stirring for 3 min), 1.4 ml of 10 mM hydroxylamine hydrochloride solution (stirring for 8 min) and 90 µl of 10% w/v $HAuCl_4$ (added dropwise, 1 drop per second). The concentration of 30 nm, 55 nm, 90 nm and 120 nm AuNPs suspensions is 9 10^{-11} mol l^{-1}, 6 10^{-11} mol l^{-1}, 8 10^{-12}, mol l^{-1}, 6 10^{-12} mol l^{-1} respectively. The suspensions were kept in continuous stirring overnight at room temperature in the dark before using it.

2.3. Gold nanoparticles characterization

AuNPs characterization was done by UV–Vis absorption measurements and by Scanning Electron Microscopy (SEM) imaging. UV–Vis absorption spectra were collected in the range 400–1100 nm with the Evolution 60s spectrophotometer (Thermo Scientific). The wavelength resolution is 1 nm. SEM characterization was carried out using a SEM FEI Inspect F in UHV mode with the secondary electrons (SE) detector. Typical settings for the imaging are: 10 kV accelerating voltage, 2.5 electron beam spot (18 pA) or 3.5 spot (30 pA), 10 mm WD. By imaging the particles using SEM, size and shape of AuNPs were characterized as well as the size distribution of their particles. At least 300 nanoparticles were counted for each sample to estimate the mean diameter and the relative standard deviation of the AuNPs.

2.4. Preparation of pyrimethanil standard suspensions and solutions

Pyrimethanil solubility in water at room temperature is 0,121 g/l; in case of higher concentration it is dispersed in a stable suspension. Pyrimethanil stock standard suspension was prepared by accurately diluting 2 ml of Scala® (400 g l^{-1} of Pyrimethanil suspension) in 100 ml and 200 ml of Milli-Q water, to reach a concentration of 8 g l^{-1} ($8*10^3$ ppm) and 4 g l^{-1}. Pyrimethanil standard solutions were prepared by subsequent dilutions from the stock suspensions in water to reach the following concentrations: 40 mg l^{-1}, 30 mg l^{-1}, 20 mg l^{-1}, 10 mg l^{-1}, 5 mg l^{-1}, 1 mg l^{-1}. These pure pyrimethanil standards were used for AuNPs aggregation test, SERS efficiency test and to set up the analytical procedure.

2.5. AuNPs aggregation test

Aliquots of pyrimethanil standard suspension (400 mg l^{-1}) were mixed in a 1:2 ratio with AuNPs stock suspension, mixed with vortex for 3 s and subsequently analyzed by UV–Vis. In these conditions PMT is in high excess with respect to AuNPs and their interaction, if present could not be negligible. Measurements in acidic conditions were performed after adding few drops of 1 M HCl to reach a pH value close to 3. UV–Vis measurements were repeated over four days.

2.6. SERS efficiency test

1 µl of a 400 mg l^{-1} pyrimethanil standard suspension was deposited by drop casting on a flat gold surface and let it dry in air for evaporation. 5 depositions were performed on the surface in order to obtain an array of 5 pyrimethanil spots (4 spots for SERS collection and 1 spot for normal Raman reference collection). Each spot was covered with 2 µl of AuNPs for Raman mapping after drying. A reference spot for SERS analysis was also made by covering a PMT spot with 2 µl of water. The concentration of all AuNPs suspension was levelled to have the same exposed surface area ($4 * 10^{12}$ nm^2), avoiding bias in case of larger NPs.

2.7. Detection of PMT on pome fruits

Pome fruit samples such as green apples were bought from a local store. The whole fruit was washed with sodium bicarbonate to remove contaminants from the surface and then spiked with different amount of PMT standard suspensions. For the on-peel detection tests, the spiking procedure was set using a manual nebulizer with 100 ml capacity in order to better simulate the in-field pesticide diffusion on fruits. For the accurate contamination of the sample to be used as validation test of the quantitative method, the PMT suspension was deposited using a micro syringe with a 0.1 µl precision.

In situ detection of pyrimethanil was performed by depositing 2 µl of a 10-fold concentrated 120 nm AuNPs suspension on the contaminated peel, followed by Raman mapping after the evaporation of the colloids suspension. The 10-fold concentrated 120 nm AuNPs suspension was obtained by centrifugating the AuNPs stock suspension at 600 g for 12 min and subsequently re-suspending in a proper amount of water suspension.

For an accurate and precise quantification of the fungicide on the entire surface of the fruit, an extraction procedure was carried out by thoroughly rinsing the contaminated peel with a known amount of distilled water (usually equal to the fruit weight) to recover pyrimethanil from the surface. Three separated rinses using one third of the total washing volume were performed to increase the extraction efficiency. 2 µl of the resulting solution were deposited by drop casting on a silicon dioxide surface and let them dry in air for evaporation. 2 µl of a 10-fold concentrated 120 nm AuNPs suspension were then deposited on the PMT spot and analyzed by Raman mapping after drying. The content of PMT in real samples was determined by SERS according to the analytical procedure reported in Section 2.9.

2.8. SERS measurement

SERS spectra were recorded using a Thermo Scientific DXR Raman equipped with a microscope, excitation laser source at 780 nm, a motorized microscope stage sample holder, and a charge-coupled device (CCD) detector. Raman equipment is monthly calibrated through a software-controlled calibration tool which ensures wavelength calibration using multiple neon emission lines, laser frequency calibration using multiple polystyrene Raman peaks, intensity calibration using standardized white light sources. The frequency uncertainty is determined by the grating resolution of 5 cm−1 (the grating groove density is 1200). The intensity uncertainty was demonstrated to be lower than 5% using a polystyrene standard. Spectra of samples were collected using a 20x long working distance microscope objective (spot size 1.7 µm, N.A. 0.40) with a 10 mW laser power and a spectral range from 150 to 3400 cm^{-1}. The acquisition time for each spectrum was 1 s for 5 exposures. A Raman map of about 25 spectra was collected on each PMT-AuNPs spot (about 0.5 mm^2 area was investigated) and the obtained spectra were averaged for statistical analysis.

2.9. Computational procedure

Geometry optimization of model PMT structures and consequent calculations of vibrational (IR and Raman) spectra were carried out with DFT method using Gaussian 03 program (Gaussian 03, Revision B.05, References cited in http://www.gaussian.com). Full geometry optimizations were carried out without symmetry constraints. The computations were performed with the Lee, Yang and Parr correlation

functional (LYP) (Lee, Yang, & Parr, 1998) combined with the Becke's non-local three-parameter hybrid exchange functional, (B3) (Becke, 1993). Vibrational information coming from the computational procedure were compared with the experimental Raman spectrum of PMT and the main bands in the spectrum were assigned using the Handbook of Infrared and Raman Spectroscopy (Socrates G "Infrared and Raman Characteristic Group Frequencies: Tables and Charts", Wiley ISBN: 978-0-470-09307-8).

2.10. Quantitative calibration and validation of the method

The instrumental linearity was evaluated from a calibration curve calculated with five levels of PMT concentrations in non-spiked fruit extract, representative of the analyzed matrix: 0 mg kg^{-1}, 5 mg kg^{-1}, 10 mg kg^{-1}, 20 mg kg^{-1}, 40 mg kg^{-1}. 2 µl of each PMT standard solution were deposited by drop casting on a silicon dioxide surface and let them dry in air for evaporation. In the calibration procedure of SERS analysis, 2 µl of a 10-fold concentrated 120 nm AuNPs suspension were deposited on the five spots with increasing concentrations of pyrimethanil. After drying, Raman mapping was performed on each spot, as described in Section 2.8, and all spectra from each map were averaged for statistical analysis. Each measurement was repeated 4 times to test measurement repeatability for a total of 20 calibration standards. A specific AuNPs Raman band at 2130 cm^{-1} was exploited to normalize the Raman intensity of pyrimethanil spectrum, minimizing possible variations due to laser power, focal distance and environmental parameters (temperature, humidity) and to overcame variations of the enhancement effect due to the different ratio between the amount AuNPs and analyte molecules. The uncertainty of pyrimethanil concentrations was also calculated, as recommended by the GUM JCGM 100:2008 and Supplement 1 JCGM 101:2008, in order to meet metrological requirements. The intensity of PMT Raman band at 997 cm^{-1} was plotted versus pyrimethanil concentration to obtain the calibration curve. The applied fitting procedure was a weighted total least square (WTLS) regression, and was implemented by means of a MATLAB®-based tool for calibration problems that is able to deal with uncertainty (and correlation) in both the dependent (average intensities) and independent (mass values) variables; the Calibration Curve Computing Software for the evaluation of instrument calibration curves is provided by the Italian national institute for metrological research (INRiM) (CCC software link, https://www.inrim.eu/research-development/quality-life/ccc-software). The linearity in the concentration range considered was estimated by the reduced chi-square value ($\chi 2$). Acceptability criterion to assume the linearity of response is a $\chi 2$ close to 1.

Multivariate calibration was performed using Partial Least Square method. PLS regression is based on the maximization of the covariance between variables (spectral frequencies) and response (contaminant concentration) associated to the calibration standards (Wold, 2006). Seven concentrations of pyrimethanil (0 mg kg^{-1}, 1 mg kg^{-1}, 5 mg kg^{-1}, 10 mg kg^{-1}, 16 mg kg^{-1} 20 mg kg^{-1}, 30 mg kg^{-1}, 40 mg kg^{-1}) were deposited and covered with AuNPs as described above. For each standard 4 SERS maps were collected and the mean

spectrum of each map was used as calibration standard for a total of 32 calibration standards. PLS calculation was performed using the PLS Toolbox for Matlab®. PLS regression was applied to mean centered SERS spectra. Spectral frequencies ranging from 180 cm^{-1} to 2500 cm^{-1} were considered, excluding the first order of silicon in the range between 500 cm^{-1} and 550 cm^{-1} that was not included in the calibration process. The optimal number of PLS latent variables was selected on the basis of the cumulative explained variance (CEV) for each component and the root mean square error in cross validation (RMECV). The validation was performed using a venetian blinds cross validation procedure with 6 cancellation segments at first for method optimization and an external set of four samples for test set final validation.

New methodologies based on ELISA (Mercader, Esteve-Turrillas, Agullo, Abad-Somovilla, & Abad-Fuentes, 2012) and electrochemical sensors (Garrido et al., 2016, Yang et al., 2015) were recently proposed as interesting alternatives to the traditional analytical methods, providing high selectivity and sensitivity in PMT detection in real samples. However, no studies were made so far concerning the development of a PMT detection tool based on Surface Enhanced Raman Scattering (SERS). Compared with the conventional analytical techniques, Raman spectroscopy allows fast detection times, high selectivity due to the Raman fingerprint of molecules and minimal or no preliminary treatment of the sample. Moreover, the sensitivity of the normal Raman technique can be increased by several orders of magnitude in SERS analysis due to the enhancement of the Raman scattering of molecules absorbed onto, or microscopically close to, a suitable plasmonically active surface, such as roughened nanostructured metal surface, or metal colloids (Schluecker, 2014). For all these reasons SERS represents a good candidate in food control analysis. Different SERS approaches were already reported on the detection of various classes of pesticides in real-food matrices. In case of solid matrices, homogenization of the peel or surface swab methods were used to recover pesticides from the surface and the detection was subsequently performed using solid surface-based substrates (Fan et al., 2014, He et al., 2014). In situ detection of pesticides in fruits was also demonstrated using different types of metal nanoparticles (NPs) (Li et al., 2010, Liu et al., 2012) which were spread as “smart dust” over the surface that has to be probed. However, even if these SERS substrates demonstrated to achieve a very high sensitivity in the detection of chemical contaminants, they usually suffer from lack of reproducibility and inconsistent performance when spot-to-spot tests are conducted, leading to problems in the quantification process. Therefore, standardized SERS tool with a good compromise between sensitivity and reproducibility of analysis are needed to provide reliable analytical methods in the detection of food contaminants.

In this work we propose a versatile, simple and reproducible procedure to detect, discriminate and quantify residues of pyrimethanil on pome fruits by SERS. We selectively tested spheroidal AuNPs with different dimensions in order to have the highest SERS effect. The analytical procedure was set up on a flat surface as model system to standardize SERS methodology for both qualitative and quantitative analysis. Raman mapping was exploited to increase signal reproducibility from spot to spot analysis and to provide more

consistent results. A semi-quantitative in situ detection method on fruit peel was assessed and an accurate method for pyrimethanil quantification on fruit surface was developed and validated.

3. Results and discussion

Several studies already proposed metallic NPs as useful substrates for pesticides detection but in most of these methods a strong chemical interaction between the colloids and the analyte occurred. This binding affinity normally leads the aggregation of the NPs generating clustered SERS hot spots which are responsible for a huge enhancement of their Raman signals. Unlike it was previously reported, the chemical structure of pyrimethanil does not support selective binding with citrate terminated AuNPs and the enhancement of its Raman signals can be exclusively promoted by the electromagnetic effect, which has to be induced by the proximity of the fungicide on the metallic NPs surface. The chemical interaction of AuNPs with pyrimethanil was initially studied performing AuNPs aggregation test in suspension. Spheroidal AuNPs with different size were fabricated, as reported in the Section 2.2, and characterized by SEM and UV–Vis measurements. SEM images of AuNPs with the mean diameter of 30 nm, 55 nm, 90 nm and 120 nm, respectively are shown in Fig. 1S in Supplementary information.

The UV–Vis absorption spectra of these NPs were acquired and they are reported in Fig. 2S in Supplementary information. As the size of AuNPs increases, the λmax was found out to increase from 530 nm to 580 nm, which agrees with the previous conclusion that the maximum peak wavelength red-shifts as the relative particle size gets bigger (Hong & Li, 2013).

The chemical interaction of AuNPs with pyrimethanil was studied by means of a AuNPs aggregation test (Fig. 1), as reported in Section 2.5. A decreased stability of the colloids in suspension would provoke the aggregation of AuNPs, inducing a shift of the localized surface Plasmon resonance (LSPR) with a consequent variation of the colloidal system color from red to blue, that can be easily monitored by UV–Vis absorption measurements.

The stability of the colloidal suspensions was monitored at acidic conditions (pH ∼ 3) in which PMT is completely solubilized in water and its interaction with citrate-terminated AuNPs should be maximized (pKa Pyrimethanil = 3.26). As Fig. 1 shows, no shift of the LSPR peaks at higher wavelengths was registered over 15 min for the 30 nm, 55 nm, 90 nm and 120 nm AuNPs colloids after adding PMT (400 mg l^{-1}), meaning that no, or very low, chemical affinity exists between AuNPs and the analyte. No shift of the LSPR peaks was further observed after four days, confirming the long term stability of all these colloidal systems in the presence of PMT (Fig. 1).

Since PMT and AuNPs do not interact in a liquid medium, PMT detection has to be conducted in dry condition in order to promote the absorption of the PMT on the AuNPs surface and to maximize the electromagnetic effect in SERS technique.

A comparative SERS efficiency test using spheroidal AuNPs with a diameter of 30 nm, 55 nm, 90 nm and 120 nm was performed to investigate the effect of the nanoparticle size on the Raman enhancement, as it was described in Section 2.6. The sum of surface area A of all AuNPs was calculated using Eq. (1), assuming that all nanoparticles are spherical (Hong & Li, 2013)

$$A = 4\pi r^2 n = \frac{6\pi d^2 m_t}{D\pi d^3} = \frac{6m_t}{Dd} \quad (1)$$

where n is the number of nanoparticles; mt is the total mass of Au in the suspension; D is the density of Au assuming that the density does not change with the size of the nanoparticles; d is the diameter of the nanoparticles.

To provide a consistent comparative study, the total surface area of AuNPs with different size was kept the same in SERS efficiency test. The total surface area was normalized to the surface area of a 10-fold concentrated 120 nm AuNPs suspension, corresponding to $4 * 10^{12}$ $nm^{2.}$

Normal Raman spectrum of PMT in solid state is shown in Fig. 2. Typical Raman fingerprint of pure PMT exhibits vibrational peaks at 560 cm^{-1}, 610 cm^{-1}, 620 cm^{-1}, 997 cm^{-1}, 1033 cm^{-1}, 1246 cm^{-1} and 1296 cm^{-1} whose assignments are reported in Fig. 2. Band assignments for PMT molecule were obtained by a combination of a computational procedure with vibrational information from Handbook of Infrared and Raman Spectroscopy, as reported in the Section 2.9 of Material and Methods.

As Fig. 3 shows, SERS spectral features of PMT standard obtained with the all tested AuNPs were consistent with its conventional Raman spectrum. The major characteristic peaks found in the Raman spectrum of PMT (560 cm^{-1}, 610 cm^{-1}, 620 cm^{-1}, 997 cm^{-1}, 1033 cm^{-1}) were clearly visible in their SERS spectral counterparts. However, the relative intensities of characteristic peaks may change, broadening of peaks may occur, and new peaks may show up in the SERS spectra. For example, intensity of the characteristic double peak of PMT at 610 cm^{-1}, 620 cm^{-1} was increased, the peak at 560 cm^{-1} was broadened and a new peak at 950 cm−1 showed up in SERS spectra compared to its conventional Raman spectrum. These changes were due to the interactions of analyte molecules with the surfaces of gold nanoparticles, in particular related to the orientations of analyte molecules on the substrate surface and the specific functional group(s) of the molecules bound to the substrate (Luo, Huang, Lai, Rasco, & Fan, 2016).

The SERS response of four different AuNPs colloids was compared with the aim to select the best enhancing system for our scope. As demonstrated in Fig. 3, all the AuNPs tested were able to enhance the specific

peaks of pyrimethanil in SERS analysis compared to the normal Raman spectroscopy. The peak at 997 cm^{-1} was used to compare the intensity of the different AuNPs because it exhibits the highest intensity and it is characteristic of the breathing mode of the PMT aromatic ring (Herzberg, 1988). The analytical enhancement factor (EF) for each size of AuNPs was calculated using (2), where ISERS and INR are the intensity of the vibrational peak in SERS and normal Raman (NR) measurements, respectively, and CNR and CSERS are the concentration of PMT in NR measurements and the SERS measurements, respectively (Kara et al., 2016):

$$EF = \frac{I_{SERS} C_{NR}}{1 + I_{NR} C_{SERS}} \quad (2)$$

The EF increases together with AuNPs size, the highest value is reached when the 120 nm AuNPs are used as reported in Table 1S in Supplementary information. It is known that the local electromagnetic enhancement increases with the increasing particle size (Kelly, Coronado, Zhao, & Schatz, 2003) and as soon as the particles get bigger also the SP band red-shifts, moving closer to the excitation wavelength of the laser (780 nm). This probably explains our observations that the SERS EF generated from AuNPs is maximized when the size of the gold NPs is around 120 nm. Moreover, we can infer that 120 nm AuNPs arrange in a more suitable morphology in terms of roughness and vicinity of NPs on the contaminated surface. Therefore, 120 nm AuNPs were selected and used for the further development of the present methodology.

In order to demonstrate a practical application in the food safety field, green apples were contaminated with PMT trace residues and in situ detection of the fungicide on a real sample was initially tested. The surface of a green apple was contaminated by depositing 1 µl of PMT concentrated suspension (40 µg of PMT) on the peel. 0.5 cm^2 area was covered approximately in order to create an ultra-contaminated zone on the peel. Normal Raman mapping was performed on the contaminated area but no or very low signals of PMT were collected on the surface even if the local concentration is 80 µg cm^{-2} (Fig. 4a). In order to increase the sensitivity of the technique, a concentrated suspension of 120 nm AuNPs was spread as “smart dust” over the contaminated area and SERS mapping was conducted. As Fig. 4b shows, the typical fingerprint of the PMT was registered after AuNPs deposition and its spatial distribution on the surface was easily monitored by the micro-mapping Raman system. A color scale bar from blue to red was associated to the intensity of the specific PMT peak at 997 cm^{-1} and related to the x,y position on the analyzed surface in order to provide a semi-quantitative information of the PMT amount on the apple peel.

Raman mapping presented in Fig. 4 clearly demonstrated that in situ detection of PMT on the apple peel only occurs when AuNPs are applied on the surface, while very low or no PMT signals were registered in the contaminated regions without AuNPs. This means that normal Raman technique is not sensitive enough to

detect low amounts of PMT on the surface which is further confirmed by an increase of the signal to noise ratio (S/N) from S/N = 1.2 for NR to S/N = 5 for SERS measurements. Therefore, this approach could be easily used to achieve in situ detection of PMT and to discriminate the type of fungicide/pesticide on the fruit surface based on the specificity of the Raman fingerprint. However, this methodology would not be reliable enough to provide a quantitative information on the entire surface of the apple due to fact that only a small portion of the surface is analyzed and the colloids tend to randomly aggregate on such inhomogeneous surfaces, such as fruits peel, leading to a lack of reproducibility when spot-to-spot tests are conducted and when different fruit specimen are compared.

In order to develop a quantitative methodology for PMT detection on the entire surface of the fruit, a simple extraction procedure was first carried out to recover pyrimethanil from the surface, as explained in Section 2.7. An external calibration was chosen to set up the analytical procedure. Five concentrations of pyrimethanil (0, 5, 10, 20, 40 mg kg^{-1}) were used for the calibration curve and deposited by drop casting on a silicon dioxide surface. Silicon dioxide was chosen as model substrate because its roughness does not contribute to the SERS effect, its surface can be easily cleaned by any organic contamination and minimal interference is provided by its Raman peaks. A concentrated suspension of 120 nm AuNPs was deposited on each PMT spot and Raman mapping was applied to scan all the surface and to overcome inhomogeneity problems. An average spectrum of each map was calculated and normalized to the AuNPs peak at 2130 cm^{-1}, which was considered as internal reference to eliminate the matrix effect, environmental parameters (temperature and humidity), instrumental settings (focal distance) and to overcome variations of the enhancement effect due to the different ratio between the amount of AuNPs and analyte molecules at each standard concentration. SERS peaks at 997 cm^{-1} of PMT standards on silicon dioxide are shown in Fig. 5a. To obtain the calibration curve, normalized SERS intensities at 997 cm^{-1} were plotted as a function of PMT concentration. A WTLS regression was used for fitting the data of PMT concentrations and Raman intensities taking into account their associated variance. The uncertainty associated with the concentration values on x axis was calculated by combining together, according to the law of uncertainty propagation, the different sources of uncertainties which affect the solution concentration (B-type contributions due to the purity of the PMT and the volume measurement). The obtained uncertainties are shown, for each point in Fig. 5b, as standard uncertainty bars (with coverage factor k = 1) parallel to the x axis. The standard uncertainty associated with y values (reported as y error bars in Fig. 5b) was calculated as A-Type uncertainty on the basis of the standard deviation of the intensities at 997 cm^{-1} within each Raman map. A linear regression was found between the normalized Raman signal at 997 cm^{-1} and the PMT concentration range between 0 and 40 mg kg^{-1}. The forcefulness of the fit was confirmed by the reduced chi-square value (i.e. the sum of the weighted squared residuals normalized by the number of degrees of freedom) which is attested close to 1 in the considered concentration range. It is worthy to mention that le linear correlation between concentration and SERS intensity is not held in wider concentration range, because saturation

effects of the SERS saturation effect are observed at higher contaminant concentration. A drastic decreasing of the enhancement factor is registered for more concentrated solutions. The LOD of the method, intended as three times the standard deviation of the blank divided by the calibration curve slope is 4.74 ppm.

However, even if the WTLS regression provided good linearity as demonstrated by low $\chi 2$ value, the calculated uncertainty for slope and intercept are 14% and 19%, respectively. These values are not negligible and they might affect the reliable quantification of PMT on real samples. Therefore, it was decided to test a multivariate approach in order to minimize the random variability associated to a single variable and to consider simultaneously the whole information contained in spectral data. A new calibration method was set up using PLS regression to increase the method stability. The plot of the cumulative variance explained (Fig. 6a) and the RMSECV (Fig. 6b) versus the number permit to determine a reasonable number of component and to define a proper model complexity. For a number of LVs higher than 8 no meaningful information is added, further LVs explain just experimental noise and random variability A "chemical-shape" is conserved in the loading until LV8 (Fig. 3S), then only random variability and experimental noise is carried by further LVs. Useful plots for the model evaluation are reported in Supplementary information (Figs. 4S, 5S). The method provides an RMSECV (root mean square error in cross validation) of 4.78 mg kg^{-1} and cumulative explained variance of 87.06 %. The model was than validated with 4 samples contaminated with a nominal PMT concentration of 16 ppm providing an RMSEP of 4.03 mg kg^{-1}. Both calibration and validation samples are shown in Fig. 6c.

In order to compare the performances of the two proposed methods, green apples spiked with PMT at 7 mg kg−1 were analyzed with both methods. The contaminant was recovered from the apple peal following the optimized washing procedure described in Section 2.7. A contamination level of 8.65 ± 4.09 mg kg^{-1} and 6.89 ± 3.06 mg kg^{-1} as an average of 4 measurements was obtained using the calibration procedures based on WTLS and PLS, respectively. Both values were in agreement with the spiked amount of PMT (7 mg kg^{-1}) on the apple, demonstrating the reliability of both methodologies. However, the mean percentage error (MPE) calculated over 5 repeated measurements was 32.8% for the univariate calibration and 18.7% for the PLS. These results confirm that PLS methodology provides higher accuracy and intra-day repeatability than univariate analysis and it is more suitable for PMT detection on pome fruits.

4. Conclusions

A sensitive and rapid method to detect, discriminate and quantify residues of the fungicide pyrimethanil on pome fruits was developed by means of AuNPs and Raman spectroscopy. Spheroidal AuNPs with different size were fabricated and tested to determine the highest enhancement factor (EF) for pyrimethanil detection. The analytical procedure was set up on a silicon dioxide flat surface, here proposed as model

system, to standardize SERS methodology for both qualitative and quantitative analysis. A Raman mapping strategy was exploited to increase signal reproducibility from spot to spot analysis and to minimize bias due to different local surface morphologies, which historically affects SERS measurements. The optimized methodology was tested on apples providing: i) a semi-quantitative in situ detection of the fungicide on the contaminated fruit surface in case of highly contaminated fruits; ii) a metrological tool for pyrimethanil quantification on the entire surface of pome fruits in accordance with the European law limits. A validation set was used to define the prediction capability of the model and, most of all, to demonstrate that the multivariate approach is much worthy in case of a quantitative calibration of enhanced Raman spectra. In fact, the overall spectral features are better captured and modeled in a multivariate approach rather than in a univariate calibration, which just considers the Raman intensity at one single wavelength, leaving out all other information contained in the spectrum. Even if the present study does not cover the huge variability of natural samples and further studies are required to prove its efficacy on fruits with different surface chemistry and morphology, the method here developed guaranties sensitivity and repeatability levels compliant with the application needs and paves the new way to the calibration of quantitative methods based on SERS for tracing hazardous chemicals on non-wrinkled fruit surfaces.

Acknowledgements

The present work has been supported by EMRP project “Q-AIMDS”. EMRP in jointly funded by EMRP participating countries within EURAMET and the European Union.

Part of this work was carried out by NanoFacility Piemonte, INRiM, a laboratory supported by Compagnia di San Paolo (Italy).

References

Amvrazi, E. G., & Tsiropoulos, N. G. (2009). Application of single-drop microextraction coupled with gas chromatography for the determination of multiclass pesticides in vegetables with nitrogen phosphorus and electron capture detection. Journal of Chromatography A, 1216(14), 2789–2797.

Becke, A. D. (1993). Density-functional thermochemistry. III. The role of exact exchange.Journal of Chemical Physics, 98, 5648–5652.

CCC software link, https://www.inrim.eu/research-development/quality-life/ccc- software.

Commission Directive 2006/74/EC of 21 August 2006 amending Council Directive 91/ 414/EEC to include dichlorprop-P, metconazole, pyrimethanil and triclopyr as active substances.Evaluation of measurement

data – Guide to the expression of uncertainty in measurement, JCGM 100:2008 (GUM 1995 with minor corrections).

Evaluation of measurement data – Supplement 1 to the “Guide to the expression of un- certainty in measurement” – Propagation of distributions using a Monte Carlomethod, JCGM101:2008, http://www.bipm.org/utils/common/documents/jcgm/ JCGM_101_2008_E.pdf. Accessed 20/02/2017.

FAO/WHO, Pesticide Residues in Food 2007: Joint FAO-WHO Meeting on Pesticide Residues, ftp://ftp.fao.org/docrep/fao/010/a1556e/a1556e00.pdf, last accessed 19- 06-2017.

Fan, Y., Lai, K., Rasco, B. A., & Huang, Y. (2014). Analyses of phosmet residues in apples with surface-enhanced Raman spectroscopy. Food Control, 37, 153–157.

Frens, G. (1973). Controlled nucleation for the regulation of the particle size in monodisperse gold suspensions. Nature Physical Science, 241, 20–22.

Garrido, J. M. P. J., Rahemi, V., Borges, F., Brett, C. M. A., & Garrido, E. M. P. J. (2016). Carbon nanotube beta-cyclodextrin modified electrode as enhanced sensing platform for the determination of fungicide pyrimethanil. Food Control, 60, 7–11.

Gaussian 03, Revision B.05, References cited in < http://www.gaussian.com>.

Gilden, R. C., Huffling, K., & Sattler, B. (2010). Pesticides and health risks. Jognn-Journal of Obstetric Gynecologic and Neonatal Nursing, 39(1), 103–110.

Gonzalez-Rodriguez, R. M., Rial-Otero, R., Cancho-Grande, B., & Simal-Gandara, J. (2008). Determination of 23 pesticide residues in leafy vegetables using gas chro- matography-ion trap mass spectrometry and analyte protectants. Journal of Chromatography A, 1196, 100–109.

He, L., Chen, T., & Labuza, T. P. (2014). Recovery and quantitative detection of thia- bendazole on apples using a surface swab capture method followed by surface-en- hanced Raman spectroscopy. Food Chemistry, 148, 42–46.

Herzberg, G. (1988). Citation classic – molecular-spectra and molecular-structure. 2.Infrared and Raman-spectra of polyatomic-molecules. Current Contents – Engineering, Technology and Applied Sciences, 13 16-16.

Hong, S., & Li, X. (2013). Optimal size of gold nanoparticles for surface-enhanced Raman spectroscopy under different conditions. Journal of Nanomaterials. http://dx.doi.org/ 10.1155/2013/790323.

Kara, S. A., Keffous, A., Giovannozzi, A. M., Rossi, A. M., Cara, E., D'Ortenzi, L., et al. (2016). Fabrication of flexible silicon nanowires by self assembled metal assisted chemical etching for surface enhanced Raman spectroscopy. RSC Advances, 6, 93649–93659.

Kelly, K. L., Coronado, E., Zhao, L. L., & Schatz, G. C. (2003). The optical properties of metal nanoparticles: The influence of size, shape, and dielectric environment. Journal of Physical Chemistry B, 107(3), 668–677.

Lee, C., Yang, W., & Parr, R. G. (1998). Development of the Colle-Salvetti correlation energy formula into a functional of the electron density. Physical Review B, 37, 785–789.

Li, J. F., Huang, Y. F., Ding, Y., Yang, Z. L., Li, S. B., Zhou, X. S., et al. (2010). Shell- isolated nanoparticle-enhanced Raman spectroscopy. Nature, 464(7287), 392–395.

Li, J. F., Tian, X. D., Li, S. B., Anema, J. R., Yang, Z. L., Ding, Y., et al. (2013). Surface analysis using shell-isolated nanoparticle-enhanced Raman spectroscopy. Nature Protocols, 8(1), 52–65.

Liu, B., Han, G., Zhang, Z., Liu, R., Jiang, C., Wang, S., et al. (2012). Shell thickness- dependent Raman enhancement for rapid identification and detection of pesticide residues at fruit peels. Analytical Chemistry, 84(1), 255–261.

Luo, H., Huang, Y., Lai, K. A, Rasco, A. B., & Fan, Y. (2016). Surface-enhanced Raman spectroscopy coupled with gold nanoparticles for rapid detection of phosmet and thiabendazole residues in apples. Food Control, 68, 229–235.

Mercader, J. V., Esteve-Turrillas, F. A., Agullo, C., Abad-Somovilla, A., & Abad-Fuentes, A. (2012). Antibody generation and immunoassay development in diverse formats for pyrimethanil specific and sensitive analysis. Analyst, 137(23), 5672–5679.

Ortelli, D., Edder, P., & Corvi, C. (2004). Multiresidue analysis of 74 pesticides in fruits and vegetables by liquid chromatography-electrospray-tandem mass spectrometry. Analytica Chimica Acta, 520(1–2), 33–45.

Park, S., Lee, S. J., Kim, H. G., Jeong, W. Y., Shim, J.-H., El-Aty, A. M. A., et al. (2010).

Residue analysis of multi-class pesticides in watermelon by LC-MS/MS. Journal of Separation Science, 33(4–5), 493–501.

Raeppel, C., Nief, M., Fabritius, M., Racault, L., Appenzeller, B. M., & Millet, M. (2011). Simultaneous analysis of pesticides from different chemical classes by using a derivatisation step and gas chromatography-mass spectrometry. Journal of Chromatography A, 1218(44), 8123–8129.

Review of the existing maximum residue levels (MRLs) for pyrimethanil according to Article 12 of Regulation (EC) No 396/2005, EFSA Journal 2011, 9(11), 2454.

Rodriguez-Cabo, T., Rodriguez, I., Ramil, M., & Cela, R. (2011). Dispersive liquid-liquid microextraction using non-chlorinated, lighter than water solvents for gas chroma- tography mass spectrometry determination of fungicides in wine. Journal of Chromatography A, 1218(38), 6603–6611.

Schluecker, S. (2014). Surface-enhanced Raman spectroscopy: Concepts and chemical applications. Angewandte Chemie-International Edition, 53(19), 4756–4795.

Sharma, R. R., Singh, D., & Singh, R. (2009). Biological control of postharvest diseases of fruits and vegetables by microbial antagonists: A review. Biological Control, 50(3), 205–221.

Socrates, G. Infrared and Raman characteristic group frequencies: Tables and charts, Wiley ISBN: 978-0-470-09307-8.

Wold, H. (2006). Partial Least Squares. Encyclopedia of Statistical Sciences. http://dx.doi. org/10.1002/0471667196.ess1914.pub2.

Yang, J., Wang, Q., Zhang, M., Zhang, S., & Zhang, L. (2015). An electrochemical fun- gicide pyrimethanil sensor based on carbon nanotubes/ionic-liquid construction modified electrode. Food Chemistry, 187, 1–6.

Yu, C., Zhou, T., Sheng, K., Zeng, L., Ye, C., Yu, T., et al. (2013). Effect of pyrimethanil on Cryptococcus laurentii, Rhodosporidium paludigenum, and Rhodotorula glutinis biocontrol of Penicillium expansum infection in pear fruit. International Journal of Food Microbiology, 164(2–3), 155–160.

Zheng, J., & He, L. (2014). Surface-enhanced Raman spectroscopy for the chemical analysis of food. Comprehensive Reviews in Food Science and Food Safety, 13(3), 317–328.

Zhou, Y., Han, L., Cheng, J., Guo, F., Zhi, X., Hu, H., et al. (2011). Dispersive liquid-liquid microextraction based on the solidification of a floating organic droplet for simultaneous analysis of diethofencarb and pyrimethanil in apple pulp and peel. Analytical and Bioanalytical Chemistry, 399(5), 1901–1906.

Figures and Tables

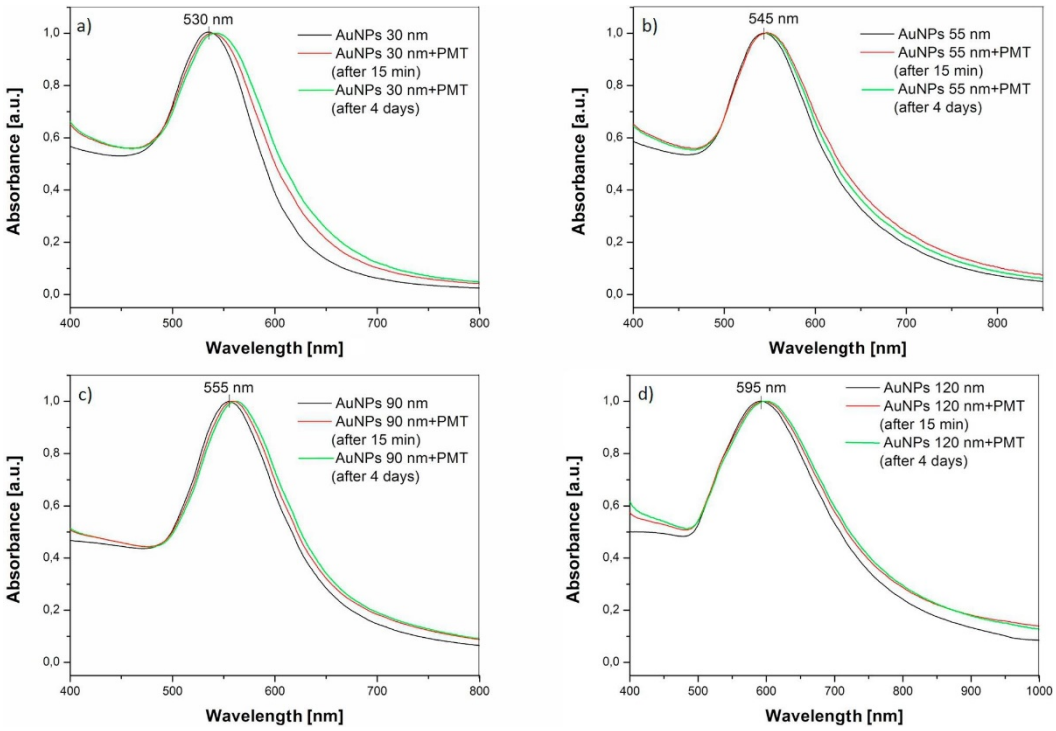

Fig. 1. UV–Vis absorption spectra of AuNPs with the mean diameter of a) 30 nm, b) 55 nm, c) 90 nm and d) 120 nm (black curves); UV–Vis spectra of AuNPs stock suspension mixed in a 2:1 ratio with pyrimethanil standard suspension 400 mg l^{-1} at pH∼3 (red curves); repetition of UV–Vis measurements after four days (green curves). (For interpretation of the references to colour in this figure legend, the reader is referred to the web version of this article.)

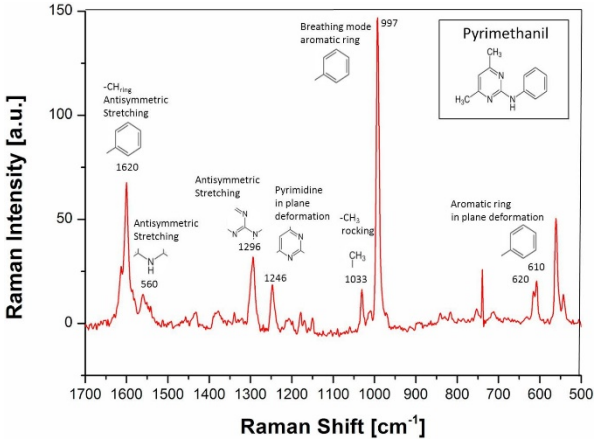

Fig. 2. Raman spectrum of pure Pyrimethanil with the characteristic vibrational peaks' assignments.

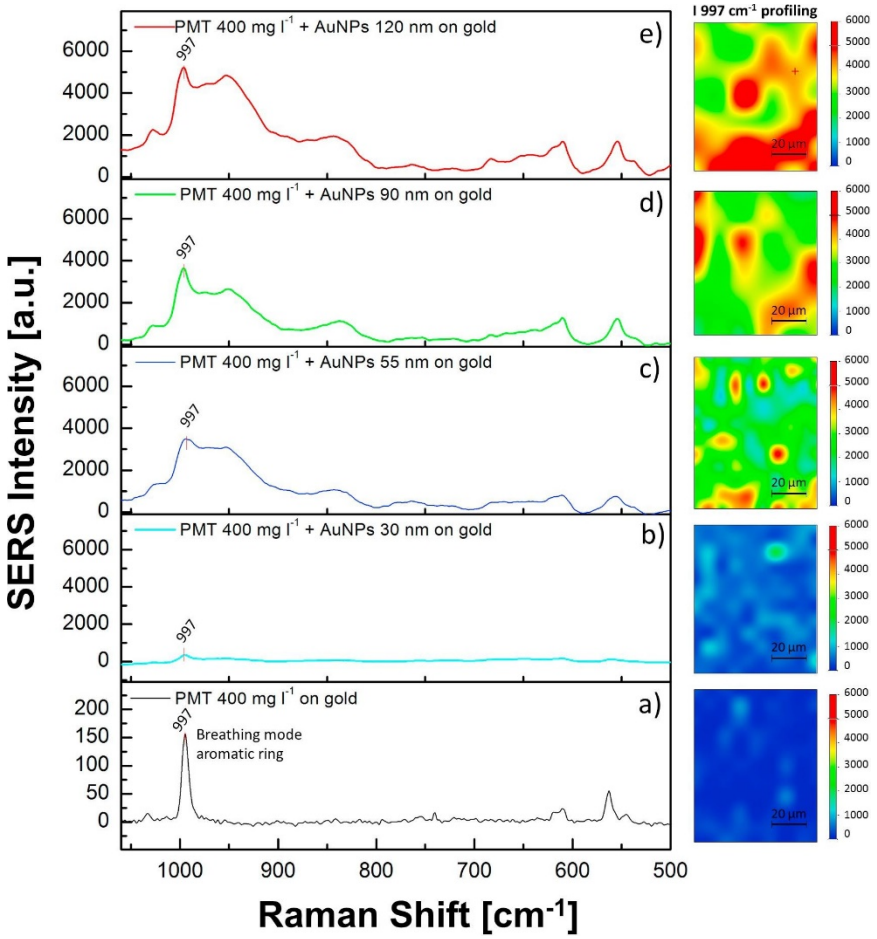

Fig. 3. a) Normal Raman spectrum of 400 mg l^{-1} PMT on flat gold surface; Representative SERS spectra of 400 mg l^{-1} PMT using AuNPs with a mean diameter of b) 30 nm, c) 55 nm, d) 90 nm and e) 120 nm on a flat gold surface. Raman mapping of each PMT-AuNPs spot was created by plotting the profile intensity of the PMT peak at 997 cm^{-1} over the scanned area with a color scale bar from blue to red. (For interpretation of the references to colour in this figure legend, the reader is referred to the web version of this article.)

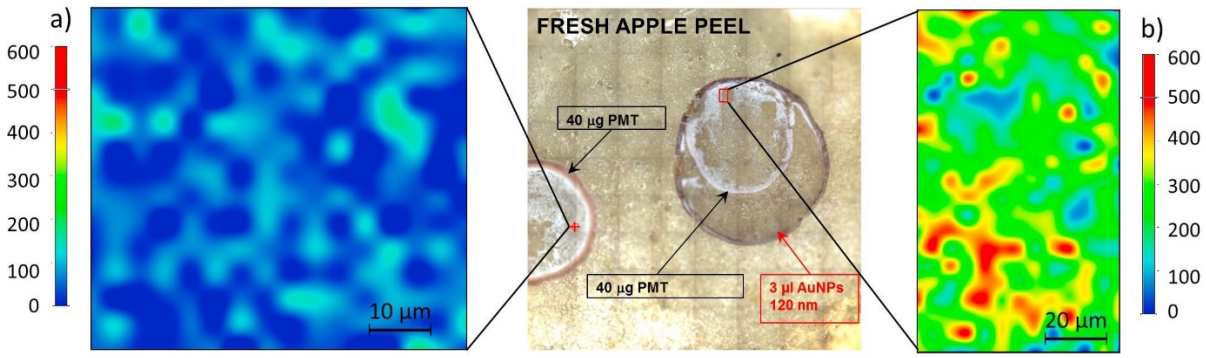

Fig. 4. a) Normal Raman mapping of PMT contaminated region on fresh apple peel; b) SERS mapping of PMT contaminated region on fresh apple peel after deposition of 120 nm AuNPs. The color scale bar for both a) and b) chemical images is related to the intensity of the PMT peak at 997 cm^{-1}.

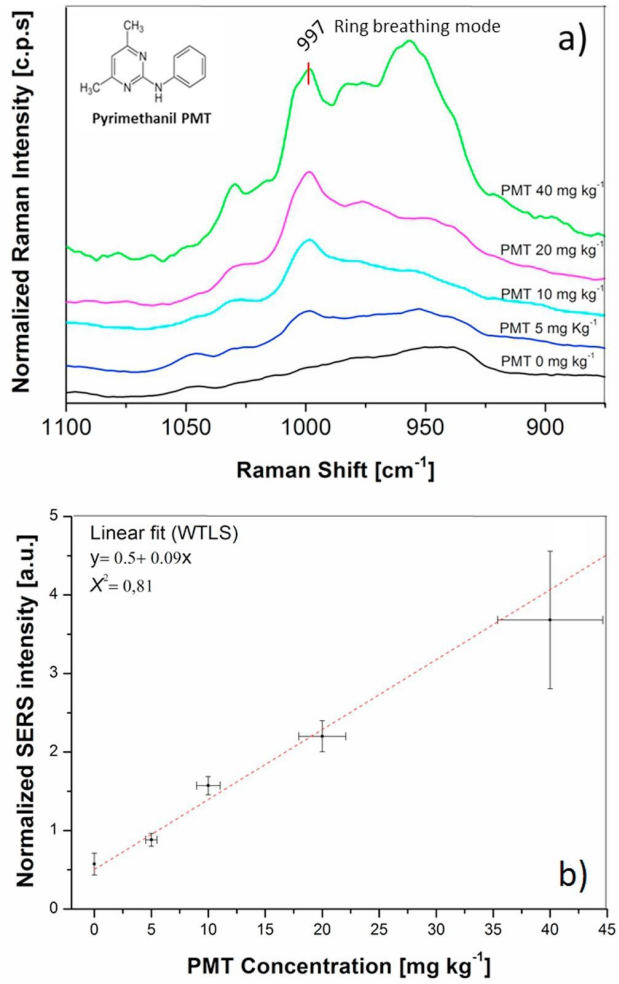

Fig. 5. a) Normalized SERS spectra of 120 nm AuNPs with 5 levels of PMT standard in negative matrix pool (representative of the analyzed matrix): 0, 5, 10, 20 and 40 mg kg^{-1}; b) Calibration curves of PMT standards in negative matrix pool obtained by plotting the normalized intensity of PMT Raman band at 997 cm^{-1} vs. PMT concentration.

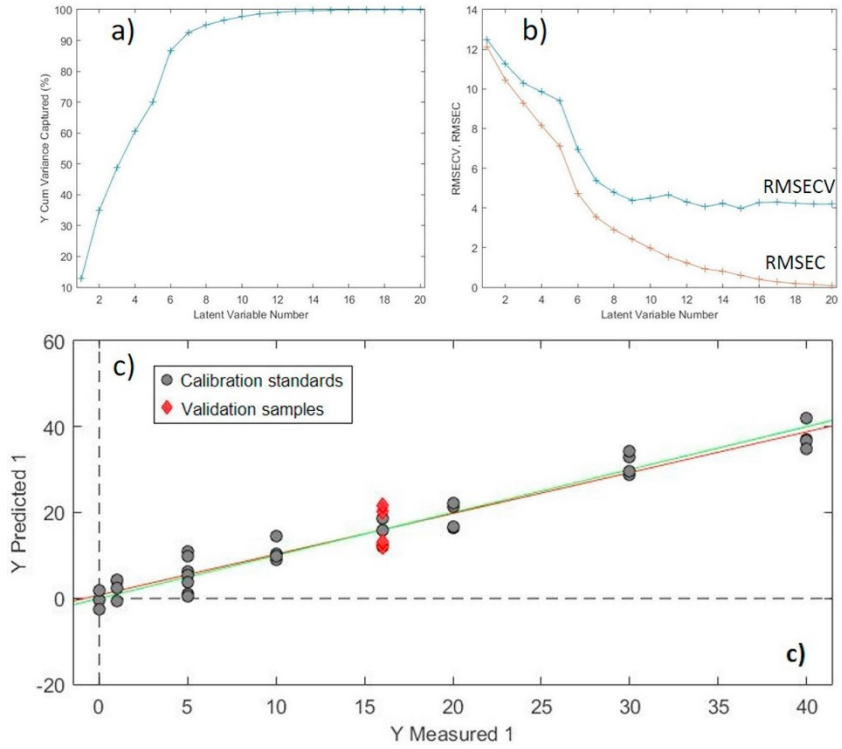

Fig. 6. PLS calibration plots: a) Cumulative Explained Variance %; b) Root Mean Square Error in Calibration and in Cross Validation versus the number of PLS latent variables; c) plot of fitted value corresponding to calibration standards (grey) and validation samples (red) versus the true values. (For interpretation of the references to colour in this figure legend, the reader is referred to the web version of this article.)